A hybrid fuzzy logic proportional-integral-derivative and conventional on-off controller for morphing wing actuation using shape memory alloy Part 2: Controller implementation and validation

T. L. Grigorie, R. M. Botez and A. V. Popov
École de Technologie Supérieure
Montréal, Québec, Canada

M. Mamou and Y. Mébarki
National Research Council
Ottawa, Ontario, Canada

ABSTRACT

The paper presents the numerical and experimental validation of a hybrid actuation control concept – fuzzy logic proportional-integral-derivative (PID) plus conventional on-off – for a new morphing wing mechanism, using smart materials made of shape memory alloy (SMA) as actuators. After a presentation of the hybrid controller architecture that was adopted in the Part 1, this paper focuses on its implementation, simulation and validation.

The PID on-off controller was numerically and experimentally implemented using the Matlab/Simulink software. Following preliminary numerical simulations which were conducted to tune the controller, an experimental validation was performed. To implement the controller on the physical model, two programmable switching power supplies (AMREL SPS100-33) and a Quanser Q8 data acquisition card were used. The data acquisition inputs were two signals from linear variable differential transformer potentiometers, indicating the positions of the actuators, and six signals from thermocouples installed on the SMA wires. The acquisition board's output channels were used to control power supplies in order to obtain the desired skin deflections. The experimental validation utilised an experimental bench test in laboratory conditions in the

Paper No. 3699(ii). Manuscript received 12 February 2011,
revised version received 2 September 2011, accepted 13 October 2011.

absence of aerodynamic forces, and a wind-tunnel test for different actuation commands. Simultaneously, the optimised aerofoils were experimentally validated with the theoretically-determined aerofoils obtained earlier. Both the transition point real time position detection and visualisation were realised in wind tunnel tests.

NOMENCLATURE

dY_1, dY_2	displacements of the two control points of the flexible skin
e	actuation loop error
FFT	fast Fourier transforms
F_{aero}	aerodynamic force
$i(t)$	command variable (electrical current in our case)
K_D	derivative gain
K_I	integral gain
K_O	change in output gain
K_P	proportional gain
LVDT	linear variable differential transducer
M	Mach number
N	perturbation global amplification factor
PID	proportional-integral-derivative
RMS	root mean square
Re	Reynolds number
SMA	shape memory alloy
t	time
Δe	actuation loop change in error
α	angle-of-attack

1.0 INTRODUCTION

Nowadays, aeronautical transport is evolving at a very fast pace, especially when compared to the beginning of the aviation era. Aeronautical traffic has tripled over the past 15 years, and by 2025, it is projected to double today's traffic volume. This traffic is expected to see an estimated +3·0% increase in the number of passengers per year, to approximately 1bn by 2016; and by 2025 the passenger increase will be accompanied by a load factor increase of 81·7% as compared to today's values[1]. This evolution will require new technological developments in the design and building of modern aircraft equipped with active control systems.

Over the same time period, fuel cost increases will lead to a slowdown in the aerospace industry, which in turn will stimulate research to find technological solutions; almost certainly in designing new fuel economy consumption methods. A new green trend has indeed started to spread out from the automobile into the aircraft industry, in which research is being carried out to reduce fuel consumption by reducing drag, which is directly related to the airflow type around the aerodynamic aircraft body design. The drag reduction concept is connected to the laminar flow and to the displacement of the transition point between laminar and turbulent flows towards the trailing edge.

Numerous studies show that the transition between laminar and turbulent flows is influenced by the shape of the wing aerofoil[2-14]. Aerodynamic studies from the beginning of aviation history

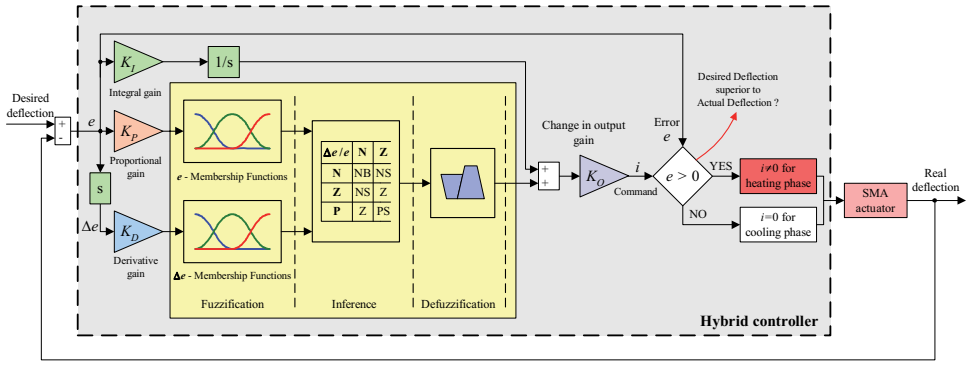

Figure 1. Hybrid controller architecture.

show that for flight conditions characterised by given Mach number (M) and Reynolds number (Re), the airflow around a wing aerofoil is laminar at the leading edge but becomes turbulent at a certain point. Turbulent flow is not desirable because it causes drag to increase, which, over time, leads to higher fuel consumption, and consequently, increased operating costs.

This research has been realised as part of a major project initiated and financially supported by industries and academia: the Consortium for Research and Innovation in Aerospace in Quebec (CRIAQ), the National Sciences and Engineering Research Council of Canada (NSERC), Bombardier Aerospace, Thales Avionics and the National Research Council Canada (NRC-IAR). The project's goal is to realise a theoretical and experimental aerodynamic wind tunnel study of a rectangular wing equipped with a flexible skin, smart actuators and optical sensors, which can change its shape, using an active controller, to move the position of the transition towards the wing trailing edge.

A rectangular wing model (0·54m × 0·9m) with a reference aerofoil WTEA-TE1 was manufactured. The lower part of the mechanical model is an aluminium block designed to allow space for the wiring, while the upper part has an aluminum structure equipped with a flexible skin made of composite materials (layers of carbon and Kevlar fibres in a resin matrix) and an actuation system (shape memory actuators (Ni-Ti)). A number of 35 flow conditions were established as combinations of five Mach numbers (0·2, 0·225, 0·25, 0·275, 0·3) and seven flow incidence angles (–1˚, –0·5˚, 0˚, 0·5˚, 1˚, 1·5˚, 2˚) to test the morphed structure. Starting from the reference aerofoil, 35 optimised aerofoils were designed for the airflow case combinations of Mach number and angle-of-attack.

Part I of this paper established the architecture for a hybrid fuzzy logic proportional-integral-derivative (PID) plus conventional on-off controller for the actuation lines of this morphing wing system (Fig. 1). The hybrid controller behaves as a switch between the SMA cooling and heating phases, in situations where the output current was 0A, or it is controlled by the fuzzy logic controller. The shapes chosen for the input membership functions were *s*-function, π-function, and *z*-function, and product fuzzy inference and the Sugeno center average defuzzifier were applied.

The following paragraphs present the controller implementation and its numerical and experimental validation.

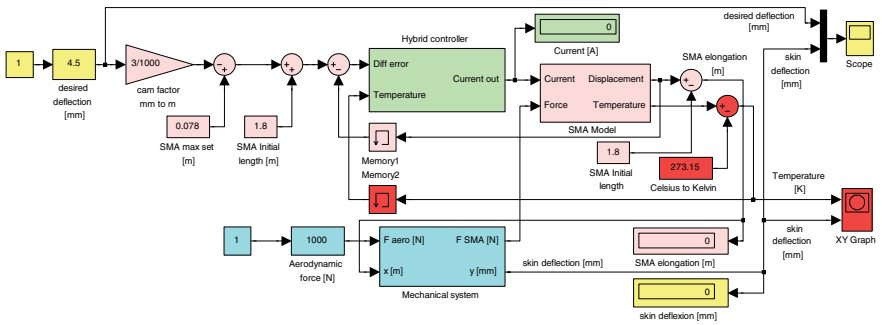

Figure 2. The simulation model for the controlled SMA actuator.

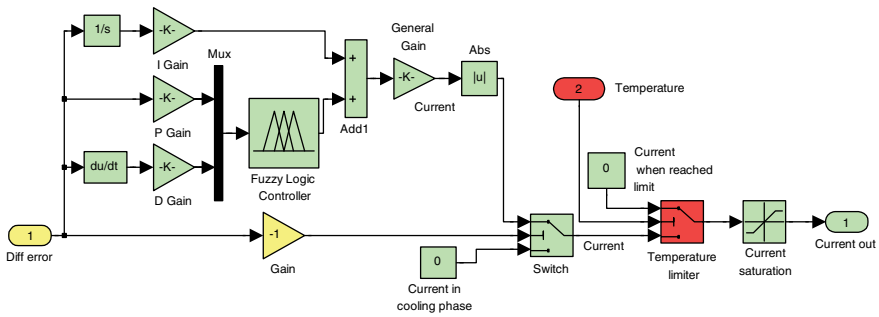

Figure 3. 'Hybrid controller' block in Simulink.

2.0 HYBRID CONTROLLER IMPLEMENTATION AND NUMERICAL SIMULATION

Introducing the controller in a block scheme, the Simulink model shown in Fig. 2 was obtained for the SMA actuators' control. The input variable of this scheme is the desired skin deflection, while the output is the real skin deflection.

The 'Hybrid controller' block in Fig. 2 implements the controller presented in Fig. 2, but also considers some aspects related to the SMA actuators' physical limitations in terms of temperature and supplying currents. The detailed Simulink scheme of this block is shown in Fig. 3. The block has as inputs the control error (the difference between the desired and the obtained displacements) and the SMA wire temperatures, and its output is the controlled electrical current applied on the SMA actuators. There are two switches in the scheme; the first switch chooses one of the two options shown in Fig. 1 (error is positive or not) and the second one switches the electrical current value to 0A when the SMA temperature value is over the imposed limit. In addition, a current saturation block is used to prevent the current from going over the physical limit supported by the SMA wires.

By estimating the aerodynamic forces for all 35 studied flight conditions and optimised aerofoils, it was possible to achieve a balance between the aerodynamic forces and the preloaded forces of the gas spring. The preloaded forces on the gas springs in the two actuation lines must be valid for all the cases studied. Loading the simulated model with an aerodynamic force F_{aero}

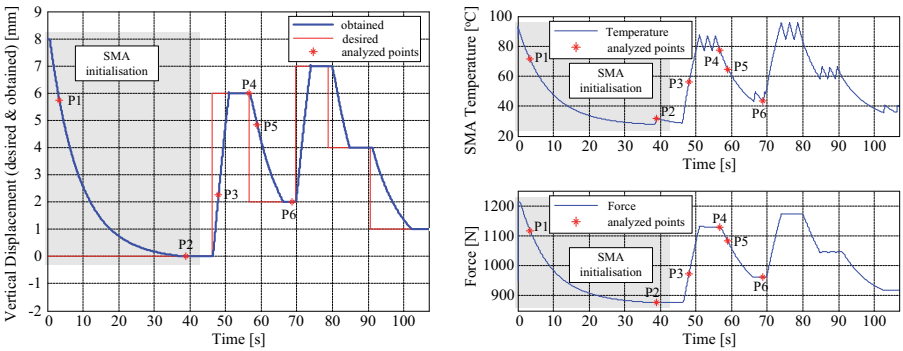

Figure 4. Response for a successive steps input when F_{aero} = 1,150N.

= 1,150N, and considering a value of 1,250N for the pretension force of the gas springs in 'Mechanical system' Simulink block (see Fig. 2), for a successive steps signal applied to the input of the controlled actuator results in the characteristics shown in Fig. 4.

The numerical simulation results shown in Fig. 4 confirm that the designed hybrid controller works very well; the variant of on-off controller combined with a fuzzy PID controller gives very good results in both phases (heating and cooling) of the SMA actuators. A few seconds of easier latency in the time of the cooling phase with respect to the heating phase can be seen.

In addition, it is clear that the temperature oscillations amplitude is higher with the increase in the level of the actuation temperature and that this amplitude depends on the loading SMA force.

To see how the controller works, some screenshots were taken at different times of the numerical simulation presented in Fig. 4. The screenshots (Fig. 5) highlight the fuzzy model input-output mapping of the six analysed points (P1-P6) *vis-à-vis* of the SMA temperature-elongation envelope. The chosen time values, shown in Fig. 4, are: 3·42s (P1), 38·82s (P2), 48·02s (P3), 56·63s (P4), 58·92s (P5), and 68·71s (P6). Figure 5 shows that the correspondence between the membership functions of the inputs and the membership functions of the output through the inference engine of the designed fuzzy model was correctly established. The same observation can be found by correlating Fig. 5 with the position of the analysed points in Fig. 4 and with the error e and change in error Δe sign and trend. A very interesting observation in correlating the same figures is that the SMA temperature-elongation envelope evolution (Fig. 5) is a function of the SMA loading forces (Fig. 4). When the elongation of the SMA is maintained constant by our controller, a constant value for the SMA loading force is obtained (the horizontal segments in the force diagram in Fig. 4), while the temperature oscillates within a few degrees about the equilibrium point (the horizontal segments in the SMA temperature-elongation envelope in Fig. 5).

3.0 BENCH TEST AND WIND-TUNNEL EXPERIMENTAL VALIDATION

Based on the theoretical and numerical simulations of the morphing wing system, we estimated the limits for the electrical current used to drive the actuators, correlated with the SMA temperature and SMA loading force. With this information, the project team decided to use two programmable switching power supplies AMREL SPS100-33, controlled by Matlab/Simulink

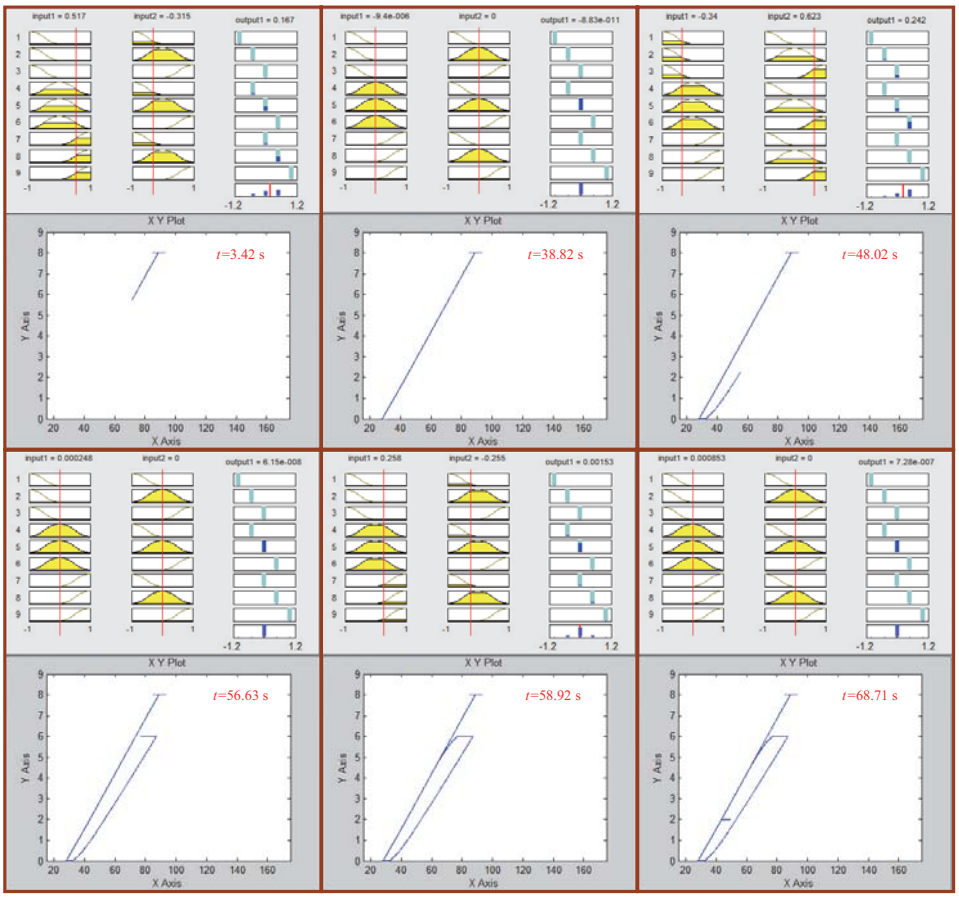

Figure 5. Fuzzy model input-output mapping of the analysed points and the SMA temperature-elongation envelope.

through a Quanser Q8 data acquisition card (Fig. 6) to implement the controller model[15-17]. The chosen power supplies have RS-232 and GPIB IEEE-488 as standard features. Among their technical characteristics are: Power 3·3kW, Voltage (dc) 0-100V, and Current (dc) 0-33A.

The Quanser data acquisition card has eight single-ended analog inputs with 14-bit resolution, which can be sampled simultaneously at 100kHz, with A/D conversion times of 2·4 μs/channel. The card is equipped with eight analog outputs, software programmable voltage ranges, which allow the control of the SMA actuators. A picture of the morphing wing system during the bench test runs is given in Fig. 7, where the actuators movement is visualised on the computer (the flexible skin was removed).

The Q8 data acquisition card was connected to a PC and programmed via Matlab/Simulink R2006b and WinCon 5.2 (Fig. 8). Two signals, from linear variable differential transformer (LVDT) potentiometers, indicating the vertical displacements dY_1 and dY_2 of the SMA actuators, and six signals from thermocouples installed on each of the SMA wires' components, were applied on the analog inputs in a single ended configuration. Two of the card output channels

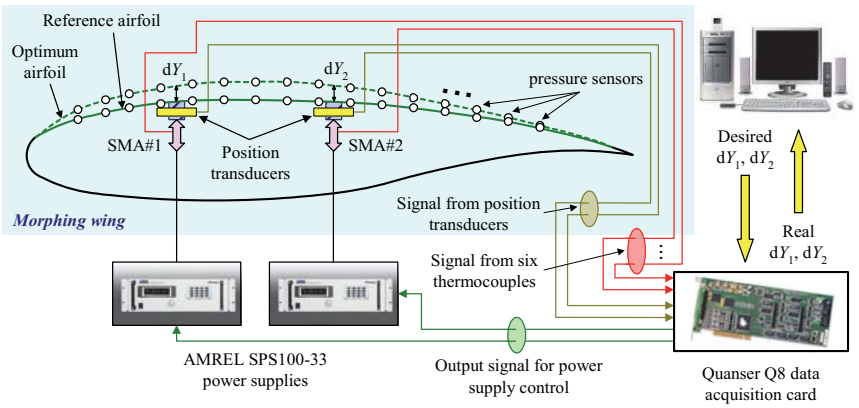

Figure 6. Bench test physical model operating scheme.

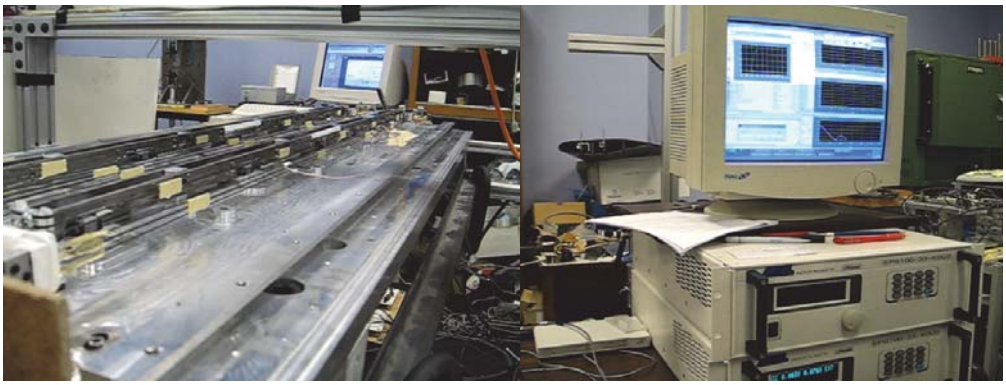

Figure 7. Morphing wing system in the bench test runs.

were used to control each power supply through analog/external control by means of a DB-15 I/O connector. As shown on the right hand side of Fig. 8, modeling the 'SMA1' block, the current supplied to the actuator was limited to 10A and the control signal was set to 0-0·606V (maximum voltage for the power supply is 2V for a 33A electrical current supply). The gas springs that maintain the SMA wires in tension have a preloaded value of 225lb (~1,000N), as in the bench test the aerodynamic force is absent. The upper limit of the SMA wires' temperature in the 'Temperature limiter' block (see Fig. 3) was established to 130˚C.

The Matlab/Simulink implemented controller was used in the same way for both actuation lines of the morphing wing system. The bench test validation of the controller started with the independent control in time for each of the two actuation lines. The desired displacements (dY_1 and dY_2), in the form of successive steps signals, were applied at the input of the actuation lines. The obtained results presented in Fig. 9 show that the controllers, in the two actuation lines, function even at zero values of the desired signal owing to the pre-tensioned gas springs. Also, small oscillations of the obtained displacements are observed around their desired values. The amplitude of the oscillations in this phase is due to the LVDT potentiometers' mechanical links

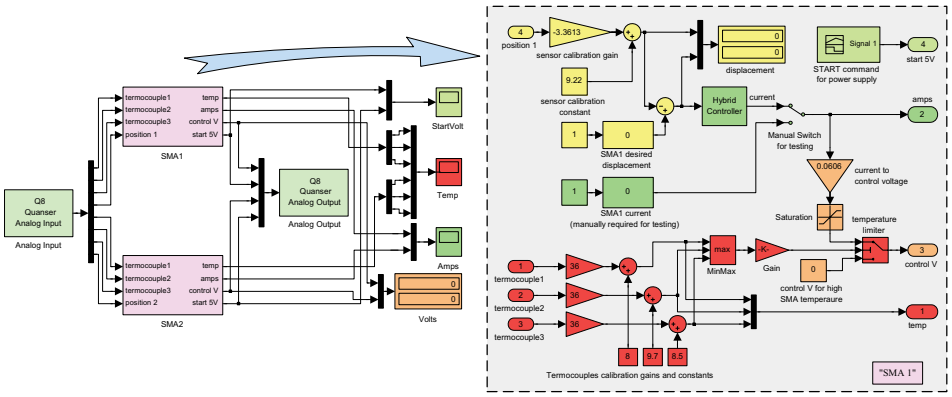

Figure 8. Matlab/Simulink actuators control during bench tests.

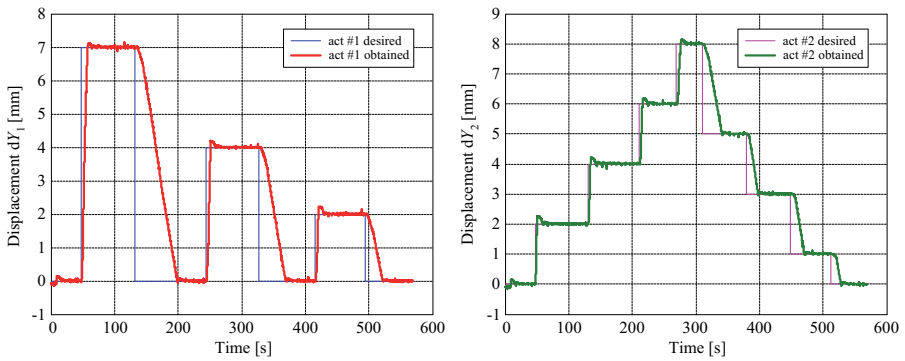

Figure 9. Bench tests for desired displacements in the form of successive steps signals.

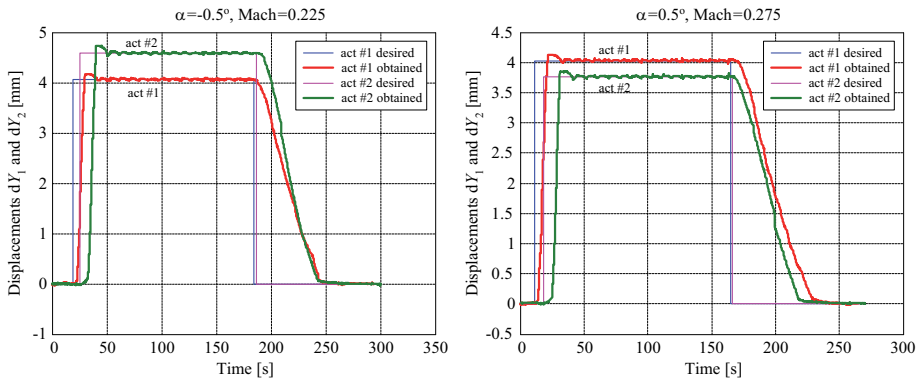

Figure 10. Bench tests for α = 0·5°and Mach = 0·225, and α = 0·5° and Mach = 0·275 flight conditions.

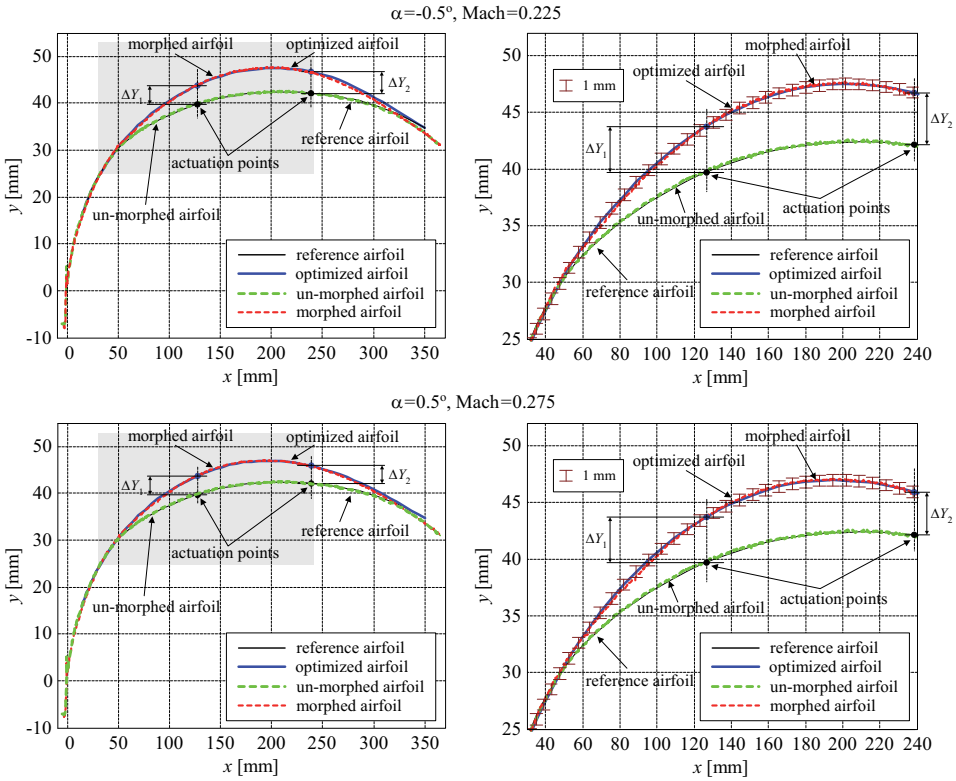

Figure 11. Theoretical versus experimental aerofoils for the cases controlled in Fig. 10.

(which were not fixed as the model was not equipped with the flexible skin in this test) and to the SMA wires' thermal inertia; the smallest amplitude is less than 0·06mm. The heating phase is more rapid than the cooling phase; heating time is of the order of a few seconds, while the cooling time is around one minute.

In the next phase of the controller bench tests validation, all pairs of the desired displacements characterising the 35 optimised aerofoil cases were imposed as input signals on the two actuation lines, while the skin was provisionally mounted on the model. The results are presented in Fig. 10 for flight conditions $\alpha = -0{\cdot}5°$, Mach = 0·225 ($dY_1 = 4{\cdot}06$mm and $dY_2 = 4{\cdot}58$mm) and $\alpha = 0{\cdot}5°$, Mach = 0·275 ($dY_1 = 4{\cdot}03$mm and $dY_2 = 3{\cdot}76$mm).

Figure 11 makes the quality of the experimental reproducibility of the theoretical reference and optimised aerofoils visible by showing the un-morphed and morphed aerofoils obtained in the two previous controlled cases; it shows the reference aerofoil, the optimised aerofoil, the un-morphed measured aerofoil and the morphed aerofoil. The characteristics on the left hand side of the figure show the entire aerofoil, while the characteristics on the right hand side present a zoom of the aerofoil between 30mm and 240mm. The experimental aerofoil co-ordinates were measured using a laser beam that scanned the center line of the wing model. The global deviation obtained for the optimised aerofoil is under 0·4mm, while in the actuation points it is under 0·05mm.

From the numerical values obtained for all 35 optimised aerofoil cases, it was observed that the position control error due to the heating-cooling cycles when the actuator maintains a desired position was less than 0·05 mm.

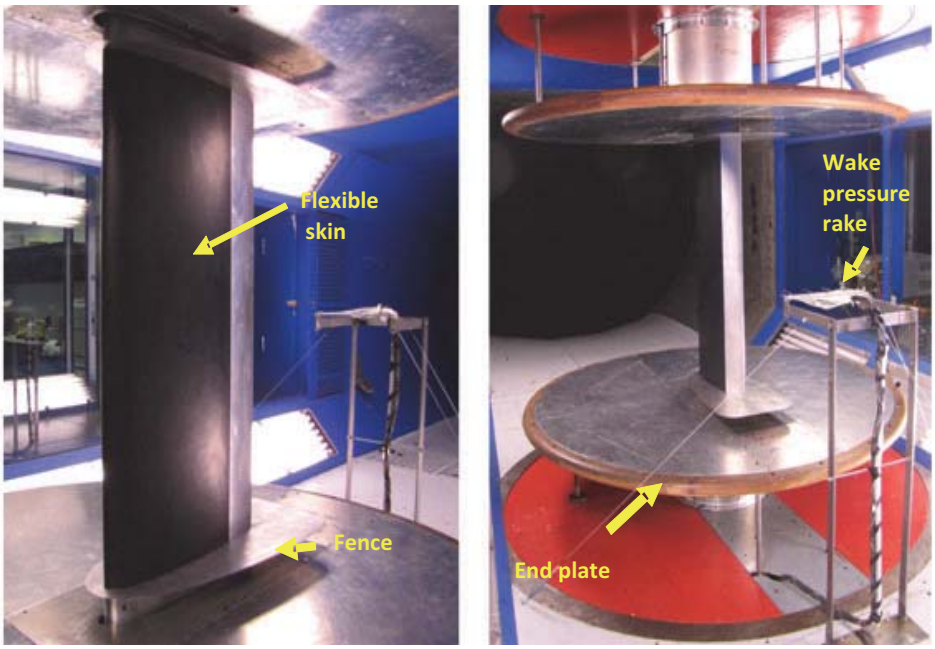

Figure 12. Wing model installed in the NRC 2m×3m wind tunnel:
(a) upper surface side view, (b) view of the model trailing edge looking upstream.

The bench test results confirmed that the experimental version of the designed hybrid controller works well in bench test conditions, where no aerodynamic forces are loaded and the preloaded gas spring's force is 1,000N.

The next step in our morphing wing project was to validate the obtained hybrid controller in a wind tunnel test. Also, by the transition point real time position detection and visualisation, in this test were validated the 35 optimised aerofoils.

A typical test for one of the 35 flight conditions consisted of a wind tunnel tare run, followed by a run for the reference (un-morphed) aerofoil, and finally a run for morphed aerofoil, reproducing the corresponding optimised aerofoil.

The controller morphed the reference aerofoil by acting on the two SMA actuation lines until the optimised aerofoil was achieved. For both test runs (un-morphed and morphed aerofoils), the transition real time location and its visualisation demonstrated the validity of all of the optimised aerofoils that had been obtained theoretically. This mechanism corresponds to the open loop architecture of the morphing wing system, when no feedback for the pressure sensors is used.

The experimental model was tested in the test section of the 2m × 3m (2m high by 3m wide) NRC atmospheric closed-circuit wind tunnel. The model setup is shown in Fig. 12(a). The wing model was mounted vertically in the wind tunnel-test section, between two circular end plates. To promote 2D-flow over the wing span, fences were incorporated at both ends of the wing, inboard of the circular end plates. A wake rake was mounted at the wing mid-span, and at a distance of 0·53m behind the model trailing edge, to measure total pressure losses, as shown in Fig. 12(b).

The wake rake consisted of 38 pitot probes and four static pressure probes, regularly spaced at 6·35mm. In most of the wind tunnel runs, 10 to 12 pitot probes were found to be located within the wing wake, and this number was judged sufficient for accurate wake drag computation.

For transition detection, 12 Kulite pressure sensors provided real-time signals, with the sensors aligned on the flexible skin along the wing chord. In this way, the IAR-NRC analog data acquisition system was connected to the pressure sensors and the acquired data were processed and visualised in real time using Matlab/Simulink software. To detect the magnitude of the noise in the surface air flow, fast Fourier transform (FFT) decomposition was used. A high-pass filtering was performed and, following the calculation of the root mean square (RMS) of the signal, the RMS was plotted to obtain the surface flow noise diagram.

In support of the discrete pressure instrumentation, infrared thermography (IR) visualisation was used to detect the transition location on the morphing wing upper surface. The transition detection method using IR is based on the differences in laminar and turbulent convective heat transfer coefficients. In the resulting images, the sharp temperature gradient separating high temperature regions and low temperature regions is an indication of the transition location. The infrared camera used was an Agema SC3000 camera, equipped with a cooled 240 × 320 pixels QWIP detector, operating in the long infrared wavelength region. The camera provided a resolution of 0·02°C and a maximum frame rate of 60Hz. It was equipped with the default lens (FOV = 20° × 15°). Optical access was provided through an opening on the side wall of the test section opposite to the upper surface[18,19].

The sampling rate of each channel of the data acquisition system was 15kS/s, which allowed a boundary layer pressure fluctuation FFT spectral decomposition of up to 7·5kHz for all channels. Following an analysis of the wind-tunnel test results, it was concluded that for the controlled morphed aerofoils the transition appeared at frequencies between 3-5kHz and the magnitudes of the pressure variations in the laminar flow boundary layer were on the order of 5e-4Pa (7·25e-8psi). The transition between laminar and turbulent flows was shown by an increase in the pressure variations, and further indicated by a strong variation of the pressure signal RMS.

For the wind tunnel tests, the preloaded forces of the gas springs were reconsidered as 1,500N because of the presence of the aerodynamic forces on the flexible skin of the wing. The control results for test run $\alpha = 1°$ and Mach = 0·225 ($dY_1 = 4{\cdot}92$mm, $dY_2 = 7{\cdot}24$mm) are shown in Fig. 13. The results obtained by the transition monitoring for this test run are shown in Fig. 14.

The FFT of the pressure signals obtained from the 12 pressure sensors are indicated in the upper plot area of Fig. 14, while the lower plot area of Fig. 14 shows the *N* factor (perturbation global amplification factor) for both aerofoils (reference and optimised), respectively the normalised RMS for 12 pressure sensors. *N* factor is derived from *eN* criterion used in X_{Foil} software, which is a much simplified way to predict the transition from laminar to turbulent boundary layer flow.

From the experimental results, a high-frequency noise appears to be influencing the LVDT sensors and the thermocouple's instrumentation amplifiers. The noise sources are the wind tunnel vibrations and the instrumentation electrical fields. Even with this noise, the amplitudes of the actuation errors (the difference between the experimental and the desired deflections) are less than 0·05mm, which does not affect the transition location – which is stable on a sensor with a high RMS spike. The left column of Fig. 14 presents the results for the reference aerofoil, and the column on the right shows the results for the optimised aerofoil. The spike of the RMS suggests that there is turbulence on sensor no. 10, near the wing trailing edge. The same result can be observed by a comparative study of the FFT curves for un-morphed and morphed aerofoils.

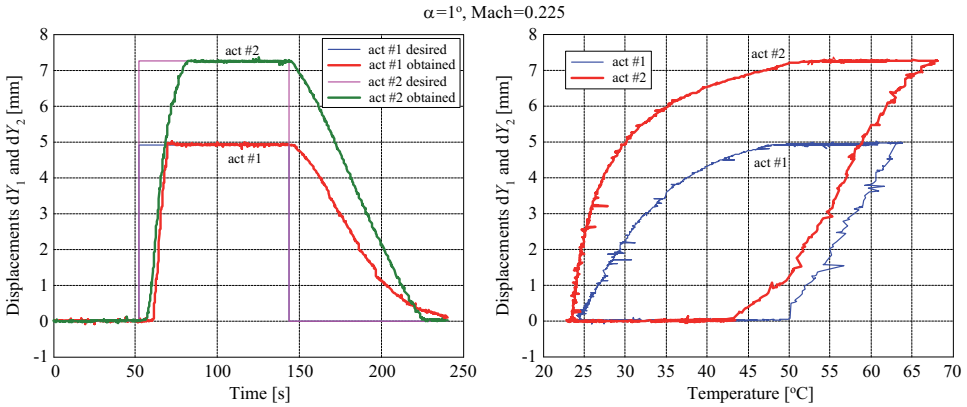

Figure 13. Wind-tunnel test for α = 1° and Mach = 0·225.

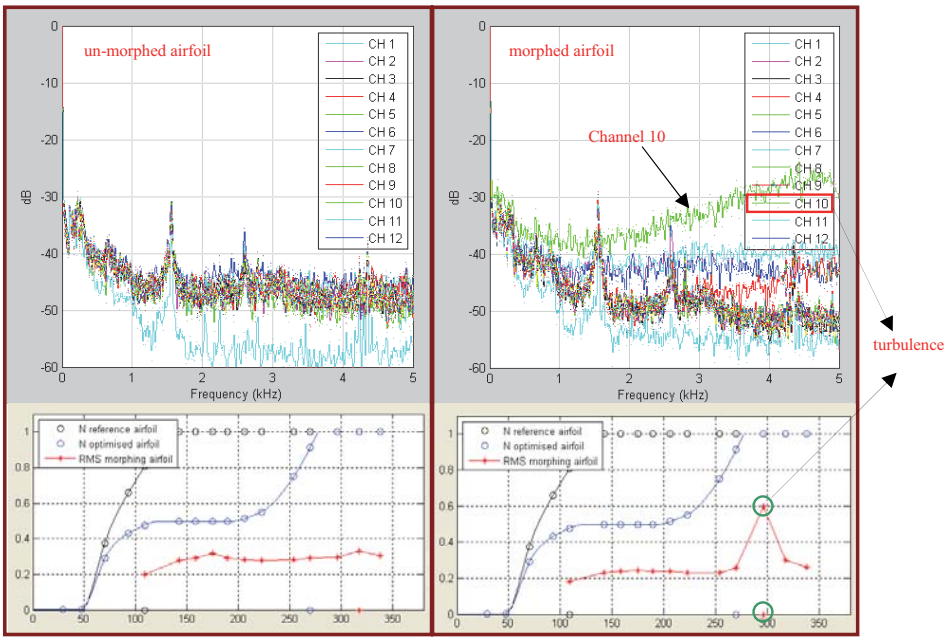

Figure 14. Transition point real-time position detection and visualisation.

As can be seen in Fig. 13, the designed controller works very well in the wind tunnel, being positively influenced by the aerodynamic forces presence. A positive impact of the aerodynamic forces presence was also observed in the reduced values of the SMA wires' work temperatures with respect to those for the numerically simulated and bench tested cases. The decrease of these temperatures is beneficial, considering the negative impact of a strong thermal field on the other system components, especially on the flexible skin and on the pressure sensors.

The infrared measurements were used to support the transition prediction obtained from the Kulite pressure transducers and to visualise the extent of the laminar flow on the wing upper

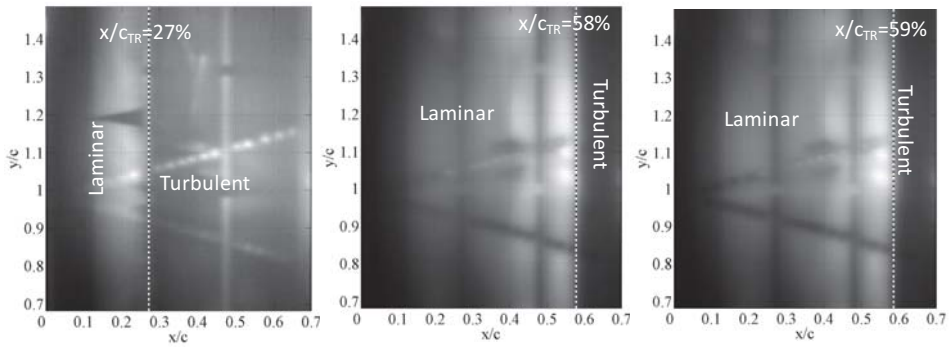

Figure 15. Infrared measurements of the transition location on the flexible portion of the wing upper surface for M = 0·275, α = 0·5°, various control methods: (a) no control, (b) open-loop, (c) close-loop. Transition location (x/c_{TR}) highlighted with dotted line and given in images (in %). Flow is from left to right.

surface for the various control configurations. Figure 15 shows typical infrared results obtained at M = 0·275 and α = 0·5° for various control methods. The white spots on the wing are the electronically heated Kulite pressure transducers. The two lines of SMA actuators, hotter or colder than the model surface, are also visible at quarter chord and near mid-chord. The locations of the transition in the images have been highlighted using a white dashed line: it corresponds to the location of a sudden surface temperature gradient, the laminar region being generally 2°C hotter than the turbulent region. The reference aerofoil configuration (Fig. 15(a)) showed a transition location at x/c = 27%. The open loop control (Fig. 15(b)) allowed a transition location at x/c = 58%. In the case of the closed loop control using fuzzy logic, (Fig.15(c)), the transition location was x/c = 59%, which is sensibly equivalent to the open loop control, considering the error on the infrared transition detection (1% x/c at 2s).

4.0 CONCLUSIONS

The approaches for the validation of a hybrid fuzzy logic proportional-integral-derivative plus conventional on-off controller used in the actuation of a morphing wing were presented.

The Matlab/Simulink numerical simulation results confirm that the obtained hybrid controller works very well. A few seconds of easier time latency in the cooling phase vis-à-vis the heating phase was noted. Also, the amplitude of temperature oscillations was observed to increase with an increase in the actuation temperature level, and depending on the load SMA force.

The bench test validation of the controller started by considering the independent control in time for each of the two actuation lines. In this way, the two desired displacements (dY_1 and dY_2) in the form of successive step signals were applied at the inputs of the actuation lines. The results obtained during this validation phase showed that the controllers in the two actuation lines functioned even at zero values of the desired signal because of the gas springs' pre-tension. Small oscillations of the obtained displacements were observed around their desired values. The amplitude of the oscillations in this phase have as principal explanations the LVDT potentiometers' mechanical links (which were not completely fixed because the model was not equipped with the flexible skin during this test) and the thermal inertia of the SMA wires.

In the next phase of the controller bench test validation, all pairs of the desired displacements characterising the 35 optimised aerofoil cases were imposed, such as input signals on the two

actuation lines, while the skin was mounted on the model. For each of the experimentally obtained aerofoils, the co-ordinates were measured using a laser beam that scanned the center line of the wing model. The global deviation obtained for the optimised aerofoil was found to be under 0·4 mm. From the numerical values obtained for all 35 optimised aerofoil cases, we observed that the position control error due to the heating-cooling cycles when the actuator maintains a desired position was less than 0·05 mm.

In the next validation step, a wind tunnel test was performed. Simultaneously, using the hybrid controller, the 35 theoretically obtained optimised aerofoils were experimentally validated, making it possible to detect and visualise the transition point real-time position. The experimental results indicated a high-frequency noise that was influencing the LVDT sensors and the thermocouple's instrumentation amplifiers. Wind tunnel vibrations and the instrumentation's electrical fields were identified as the sources. Even with these noises, the amplitudes of the actuation error (the difference between the realised deflections and desired deflections) were less than 0·05mm, and do not affect the transition, which is stable on a sensor with a high RMS spike. Also, a positive influence of the aerodynamic forces' presence on the designed controller was observed in the reduced values of the SMA wires' work temperatures compared to those for the numerically simulated and bench tested cases. The decrease of these temperatures is beneficial considering the negative impact of a strong thermal field on the other system components, especially on the flexible skin and the pressure sensors.

The infrared measurements were used to validate the pressure sensor – based transition detection method. Comparisons of the open loop and closed loop controls using the infrared results have shown that both approaches were very effective in delaying the transition location, thus reducing the skin friction drag, as confirmed by the wake rake drag measurements.

As a general conclusion, the designed hybrid controller fully satisfied the requirements imposed to achieve the purpose of our morphing wing project.

Future work on this project will focus on developing a closed loop control, based on the pressure information received from the sensors and on the transition point position estimation. Closed loop control will certainly include, as an internal loop, the actuation lines' controller presented here.

ACKNOWLEDGEMENTS

The authors would like to thank the Consortium for Research and Innovation in Aerospace in Quebec (CRIAQ), Thales Canada and Bombardier Aerospace for their financial and technical support. The authors also wish to express their appreciation to Mr George Henri Simon for initiating the CRIAQ 7.1 project and to Mr Philippe Molaret from Thales Canada for their collaboration in this work.

REFERENCES

1. SHELLABARGER, N. *National Forecast Overview 2008-2025*, 2008, Director Aviation Policy and Plans, Federal Aviation Administration.
2. BARRETT, R. Improvements to commercial and general aviation via adaptive aerostructures, 2007, Paper AIAA-2007-7873, Seventh AIAA Aviation Technology, Integration and Operations Conference (ATIO), pp 1-9, 18-20 September, 2007.
3. BYE, D.R. and MCCLURE, P.D. Design of a morphing vehicle, 2007, Paper AIAA-2007-1728, pp 321-336.

4. JACOB, J.D. Aerodynamic flow control using shape adaptive surfaces, 1999, ASME Paper No. DETC99/VIB-8323, ASME 17th Biennial Conference on Mechanical Vibration and Noise, Symposium on Structronics, Mechatronics, and Smart Materials, September 1999, Las Vegas, NV.
5. MARTINS, A.L. and CATALANO, F.M. Viscous drag optimization for a transport aircraft mission adaptive wing, 1998, ICAS-98-31499, Melbourne, Australia.
6. MUNDAY, D., JACOB, J. D. AND HUANG, G. Active flow control of separation on a wing with oscillatory camber, 2002, , Paper AIAA-2002-0413, 40th AIAA Aerospace Sciences Meeting, Reno, NV.
7. NAMGOONG, H., CROSSLEY, W. and LYRINTZIS, A.S. Morphing airfoil design for minimum aerodynamic drag and actuation energy including aerodynamic work, 2006, AIAA Paper 2006-2041, pp 5407–5421.
8. NEAL, D. A., FARMER, J. and INMAN, D. Development of a morphing aircraft model for wind tunnel experimentation, 2006, Paper AIAA-2006-2141, pp 6443-6456.
9. PINKERTON, J.L. and MOSES, R.W. A feasibility study to control airfoil shape using THUNDER, 1997, NASA Technical Memorandum 4767, Langley Research Center, Hampton, VA, USA.
10. RODRIGUEZ, A.R., Morphing aircraft technology survey, 2007, Paper AIAA-2007-1258.
11. SANDERS, B., EASTEP, F. and FOSTER, E. Aerodynamic and aeroelastic characteristics of wings with conformal control surfaces for morphing aircraft, *J Aircr*, 2003, **40**, (1), pp 94-99.
12. SKILLEN, M.D. and CROSSLEY, W.A., Developing response surface based wing weight equations for conceptual morphing aircraft sizing, 2005, Paper AIAA-2005-1960, pp 2007-2019.
13. SOBIECZKY, H. and GEISSLER, W. Active flow control based on transonic design concepts, 1999, DLR German Aerospace Research Establishment, AIAA Paper 99-3127.
14. VOS, R., DE BREUKER, R., BARRETT, R. and TISO, P. Morphing wing flight control via postbuckled precompressed piezoelectric actuators, *J Aircr*, 2007, **44**, (4), pp 1060-1067.
15. KIRIANAKI, N.V., YURISH, S.Y., SHPAK, N.O. and DEYNEGA, V.P. *Data Acquisition and Signal Processing for Smart Sensors*, 2002, John Wiley & Sons.
16. PARK, J. and MACKAY, S. Practical data acquisition for instrumentation and control systems, 2003, Elsevier, UK.
17. AUSTERLITZ, H. *Data acquisition Techniques Using PCs*, 2003, Elsevier, USA.
18. MÉBARKI, Y., MAMOU, M. and GENEST, M. Infrared measurements of transition location on the CRIAQ project morphing wing model, 2009, NRC LTR- AL-2009-0075.
19. MAMOU, M., MÉBARKI, Y., KHALID, M., GENEST, M., COUTU, D., POPOV, A.V., SAINMONT, C., GEORGES, T., GRIGORIE, L., BOTEZ, R.M., BRAILOVSKI, V., TERRIAULT, P., PARASCHIVOIU, I. and LAURENDEAU, E. Aerodynamic performance optimization of a wind tunnel morphing wing model Ssubject to various cruise flow conditions, 2010, 27th International Congress of the Aeronautical Sciences (ICAS), 19-24 September 2010, Nice, France.